Accepted Manuscript

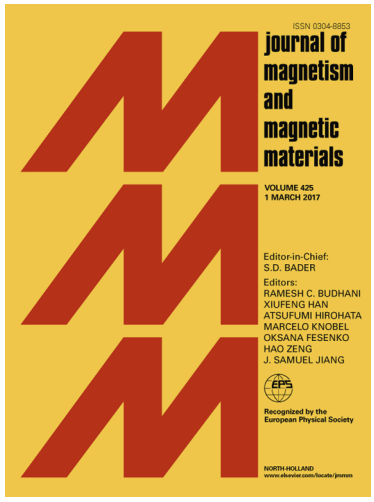

Investigation of dipolar interaction in FINEMET ribbons through longitudinally driven magneto-impedance effect

H.L. Pan, X. Li, Q. Zhang, Y.P. Su, J.T. Wang, W.H. Xie, Z.J. Zhao

PII: S0304-8853(17)32898-6
DOI: https://doi.org/10.1016/j.jmmm.2017.11.014
Reference: MAGMA 63354

To appear in: *Journal of Magnetism and Magnetic Materials*

Received Date: 12 September 2017
Revised Date: 5 November 2017
Accepted Date: 5 November 2017

Please cite this article as: H.L. Pan, X. Li, Q. Zhang, Y.P. Su, J.T. Wang, W.H. Xie, Z.J. Zhao, Investigation of dipolar interaction in FINEMET ribbons through longitudinally driven magneto-impedance effect, *Journal of Magnetism and Magnetic Materials* (2017), doi: https://doi.org/10.1016/j.jmmm.2017.11.014

This is a PDF file of an unedited manuscript that has been accepted for publication. As a service to our customers we are providing this early version of the manuscript. The manuscript will undergo copyediting, typesetting, and review of the resulting proof before it is published in its final form. Please note that during the production process errors may be discovered which could affect the content, and all legal disclaimers that apply to the journal pertain.

ACCEPTED MANUSCRIPT

Investigation of dipolar interaction in FINEMET ribbons through longitudinally driven magneto-impedance effect

H.L. Pan[1, 2], X. Li[1], Q. Zhang[2], Y.P. Su[1], J.T. Wang[2], W.H. Xie[1] and Z.J. Zhao[1]
[1] Engineering Research Center for Nanophotonics and Advanced Instrument, School of Physics and Materials Science, East China Normal University, Shanghai 200062, China
[2] National Trusted Embedded Software Engineering Technology Research Center, East China Normal University, Shanghai 200062, China
E-mail: zjzhao@phy.ecnu.edu.cn

Abstract

The magnetic dipolar interactions among multiple FINEMET ribbons have been studied by longitudinally driven magneto-impedance effect (LDMI) and hysteresis loops in this paper. The effect of dipolar fields on LDMI apparently expands the "bell" magneto-impedance profiles and raises its characteristic frequency. This is essentially correlated with the domain nucleation process under the combined effect of ac driving field and dc external field. A theoretical model was utilized to explicate the LDMI variation with the number of ribbons *N*. Basically, the nucleation field varied linearly with *N*. The influence of the frequency of ac current causes the increase of the nucleation field by adding a term $H_e \sim f^{0.38}$ before 4 MHz, but the dipolar field barely decreases with ac current. At frequency of 10 kHz, the dipolar field is fitted to be about 0.69 Oe, and the geometric factor can be estimated to be 5.60×10^{-5}. Additionally the nucleation field reduces slightly due to the compensation of the alternating field, while the LDMI ratio changes obviously. The results indicate that LDMI can be employed as a sensitive tool to reveal the dipolar interaction in FINEMET ribbons and facilitate the design of the materials for magnetic devices.

ACCEPTED MANUSCRIPT

Keywords: Dipolar interaction, Magneto-impedance, FINEMET

1. Introduction

In multi-entities magnetic system, the coupling is dominated by dipolar interaction when the distance between two magnetic entities is generally greater than the exchange interference length [1-3]. It plays a fundamental role in the formation of magnetic domains and effectively modulates their macroscopic magnetic properties, which always accompanies with a change of both the remnant magnetization and coercive/anisotropy field. This can be utilized to tune the switching fields and the sensitivity of magnetic sensors or to develop a new type of multilayer magnets [4-8]. Hence, dipolar interaction is of practical interest in the design and optimization of magnetic devices.

Generally, the dipolar interaction is studied experimentally by several conventional methods such as hysteresis loops, ferromagnetic resonance (FMR) and Mössbauer spectroscopy [9-12]. It could be theoretically calculated by utilizing the dipolar magnetization model and micromagnetism simulation [13-15]. For example, stair-like and kink-plateau-like hysteresis loops were used to calculate the dipolar fields among bistable microwires and non-bistable ribbons [9, 10], FMR frequency shift and Mössbauer spectroscopy split revealed the dipolar interaction affected deeply by the porosity of nanowires [11, 12]. In addition, MOKE and MFM were also used in the analysis of dipolar interaction among Co-rich glass-coated microwires with circular bistability and nanowires embedded in an array [16, 17]. It gave insight into the dipolar interaction influencing the magnetization behavior of multi-wires and

ACCEPTED MANUSCRIPT

simultaneously turned into an evaluation method of the dipolar field. These methods have been proven to be very useful tools in the investigation of dipolar interaction.

Apart from the aforementioned methods, the giant magneto-impedance (GMI) effect, defined as large variations in the impedance response of ferromagnetic conductors upon a dc magnetic field, has been widely exploited as a magnetic sensing technology because of its extremely high sensitivity [18-20] and also as an effective research tool for magnetic materials [21, 22]. GMI is commonly driven in transverse direction (TDMI) with ac driving current directly passing through the sensing material [23], or driven in longitudinal direction (LDMI) by means of involving a coil for sample holding and ac driving current flowing through [24]. Comparatively, the latter can conveniently avoid the welding or heat problems of the sensing materials, which is beneficial to the practical application. In a wide range of frequency, from several kHz up to GHz range, GMI can be obviously observed. At lower frequency, it is observed essentially magneto-inductance phenomenon because of negligible skin effect [25, 26]. After increasing frequency, the skin effect or energy loss caused by eddy current is the main cause of GMI [27, 28]. In addition, this effect is deeply relative to the magnetic domain structure and magnetic properties of the material itself [29]. As a research tool for magnetic materials, it could distinguish the magnetization processes in terms of domain wall displacement or domain magnetization rotation. Thus the parameters indicating the dispersion of each process, such as characteristic frequency, relaxation frequency and anisotropy field can be studied by GMI response. Moreover, these parameters are correlated with material size effect and geometrical

ACCEPTED MANUSCRIPT

structure change [30-32], which could lead to a more physical insight for understanding the dipolar interactions in multi-entities magnetic system.

In this paper, we use LDMI to measure the magnetic dipolar interactions among multiple $Fe_{73.5}Cu_1Nb_3Si_{13.5}B_9$ ribbons. In order to obtain the optimum measurement sensitivity, the amorphous ribbons are properly annealed to be FINEMET alloy for better magnetic softness. Through the analysis of the hysteresis loops and LDMI curves, we can obtain the variation of dipolar interactions with the ribbons number.

2. Experimental details

Amorphous alloy ribbons $Fe_{73.5}Cu_1Nb_3Si_{13.5}B_9$ of 0.6 mm in width, 33 μm in thickness were prepared by rapid quenching technique. The amorphous ribbons were cut to 30 mm in length and annealed at 540 °C for 20 minutes to obtain FINEMET alloys [33]. Sample specimens denoted as $(F)_N$ were composed of 1~4 overlapped FINEMET ribbons. In addition, the hysteresis loops of these specimens were tested independently by the MATS-2010SD Hysteresisgraph (HuNan Linkjoin Technology CO., LTD).

The solenoid was formed of 383-turns enameled Cu wire (ϕ=0.11 mm) wound around a ceramic tube (L=50 mm). It generated a driving field parallel to the solenoid axis. Before measuring, the specimen was freely placed in the solenoid to form an equivalent component. Then it was positioned at the center of Helmholtz Coils which produced a dc magnetic field parallel to the solenoid axis and perpendicular to the earth field direction. Its magneto-impedance was measured by using an impedance analyzer (HP4294A). The RMS value and the frequency of the ac current were varied

ACCEPTED MANUSCRIPT

from 0.3 mA~3 mA and 100 Hz~12 MHz, respectively. The relative change of magneto-impedance, i.e. the MI ratio, was defined as,

$$\frac{\Delta Z}{Z}=\frac{Z\left(H_{ex}\right)-Z\left(H_{max}\right)}{Z\left(H_{max}\right)}\times 100\% \qquad (1)$$

where $Z(H_{ex})$ and $Z(H_{max})$ are the impedance values of the equivalent component under an arbitrary and maximum external dc magnetic field (H_{max}=10 Oe), respectively.

3. Results and discussions

Fig. 1 shows the field dependence of LDMI curves for different number of FINEMET ribbons at selected frequencies (10 kHz, 120 kHz, 1 MHz and 10 MHz). The MI curves show strong dependence on the number of ribbons and the applied magnetic field. It can be observed that the ΔZ/Z spectra is a "plateau" response in low field and appears "bell" shape as a whole, which reflects a typical transverse magnetic domain structure with an easy magnetization direction perpendicular to the ribbon axis in the plane [27]. In LDMI measurement, the alternating field h_{φ} produced by the ac driving current was perpendicular to the easy axis, so the magnetization process was dominated by magnetic moment rotation. The half field width at half maximum of MI ratio in Fig. 1, H_{nuc}^{N}, was assumed to be the nucleation field of the sample $(F)_N$. The relation between the nucleation field and the anisotropy field satisfies $H_{nuc}^{N}\sim H_{k}$ [34]. After applying dc field H_{ex}, the rotation of the magnetic moment contributes slightly to the effective permeability when the field is less than the nucleation field. Then, the effective permeability μ_{eff} keeps almost constant when $H_{ex}<H_{nuc}^{N}$.

ACCEPTED MANUSCRIPT

According to the skin depth $\delta_m = \sqrt{2/\omega\mu_{eff}\sigma}$, where ω and σ is the frequency and the electrical conductivity respectively, the skin depth was invariant and no significant variations of magneto-impedance effect was observed as well. Thus, the ΔZ/Z profile was a "plateau" response in this field range. When H_{ex} is close to H_{nuc}^{N}, the magnetic moments have almost rotated to the axis direction and the moment rotation process will be impeded, resulting in the decrease of the dynamic permeability and ΔZ/Z. With further increase of H_{ex}, the remnant regions with transverse moment component are gradually diminished by H_{ex}. Hence, it leads to a monotonic decrease of μ_{eff} and LDMI ratio. Therefore, the ΔZ/Z spectra for the samples all exhibited a "bell" shape as a whole.

Fig. 2 further shows the influence of the number of ribbons and the ac driving frequency on the nucleation field. The solid symbol represents the experimental data, and the solid line is the linear fitting curves of the corresponding data. Comparatively, one can see that the value of H_{nuc}^{N} increased linearly with the number of ribbons and closely related to the driving frequency. H_{nuc}^{N} increased linearly from 0.88 Oe to 2.94 Oe at testing frequency of 10 kHz, but varied from 2.00 Oe to 3.40 Oe at 10 MHz when the number of ribbons increased from 1 to 4. Moreover, the slope S of $H_{nuc}^{N}(N)$ fitting line decreases from 0.69 to 0.46 as the frequency increased from 10 kHz to 10 MHz. This means that the slope is also influenced by the ac driving frequency.

Fig. 3 shows the maximum MI spectrum for different number of FINEMET ribbons at driving current of 2 mA. It can be seen that $(\Delta Z/Z)_{max}$ went up then down when the frequency swept from 100 Hz to 12 MHz. All the specimens $(F)_N$ have the similar

ACCEPTED MANUSCRIPT

variation. It is because the effective permeability μ_{eff} of the specimens initially increased to the maximum and then decreased with the increase of the excitation frequency [23]. From the inset of Fig. 3, it also can be seen that the characteristic frequency f_c, i.e. the frequency corresponding to the peak of $(\Delta Z/Z)_{max}$, gradually shifts to higher frequency with increasing the number of ribbons *N*. As for the peak of $(\Delta Z/Z)_{max}$ for multiple ribbons, its value is always higher than that of single ribbon. It could be ascribed to the increasing of inductive voltage on the equivalent component due to larger cross-section of inserted ferromagnetic material [19].

Fig. 4 shows the longitudinal hysteresis loops of different number of FINEMET ribbons. It can be seen that the hysteresis loop approximately shows a zero crossing oblique line. It demonstrated that the ribbons actually hold a preferential transverse magnetic domain structure and the static magnetization process was dominated by the reversible magnetic moment rotation. Simultaneously, the hysteresis loops obviously became more flattened with increasing the number of ribbons. The anisotropy field H_{k}^{N} had been obtained from the maxima of the second derivative of the hysteresis loops [35], linearly increasing from 0.75 Oe to 2.56 Oe as shown in the inset of figure 4. Comparing with Fig. 2, H_{k}^{N} was less than $H_{\text{nuc}}^{\text{N}}$ and followed the relation of $H_{\text{k}}^{\text{N}} \sim H_{\text{nuc}}^{\text{N}}$. The above discussion enables us to believe that the hysteresis loops of the specimens $(F)_N$ and its technical magnetization process should also be like as shown in Fig.4. The LDMI curve in Fig. 1 just reveals the ribbon remagnetized likewise and then the dynamic magnetization changed by the dc external field.

The reason that $H_{\text{nuc}}^{\text{N}}$ increased with *N* in Fig. 2 should be subject to the dipolar

ACCEPTED MANUSCRIPT

interactions among multiple ribbons. In order to understand the mechanism, the dipolar magnetization model is used in the following discussion. For the sample $(F)_N$, we can analyze any one of the ribbons to represent all of them. Fig. 5 describes three different magnetization states in an arbitrary FINEMET ribbon. The alternating field h_φ and the dc field H_{ex} are all parallel to the ribbon axis. In the unsaturated state of $H_{ex} < H_{nuc}^N$, including the natural state of $H_{ex}=0$ Oe, the magnetic moments will turn to a certain direction, which varies with the dc field in the range. So each ribbon cannot be simply seen as a magnetic dipole. In the saturated sate of $H_{ex} > H_{nuc}^N$, each ribbon can be treated as a magnetic dipole because the magnetic moments almost arranged in axial direction. In this state it is convenient to obtain the dipolar fields created by the neighboring ribbons. As a ribbon was magnetized by the external dc field, several superimposed dipolar fields induced by other ribbons put side by side had to be conquered. In other words, a larger dc field was needed to magnetize the moments to saturation, i.e. the nucleation field H_{nuc}^N became increasingly larger. The dipolar field of the ribbon *i* over the ribbon *j* will be [13],

$$H_{i,j} = -K_{i,j} M_i \qquad (2)$$

Where *K* is a geometric factor depending upon the size of material itself and the distance between two elements, and *M* is magnetization. Since the geometric factor $K_{i,j}$ is independent on the distance between two ribbons in a certain distance range [10, 13], the nucleation field H_{nuc}^N can be expressed as,

$$H_{nuc}^N = H_{nuc}^1 + \sum_{i=1}^{N-1} H_{i,j} = H_{nuc}^1 + (N-1)\cdot H_{i,j} \qquad (3)$$

Consequently, H_{nuc}^N is directly proportional to *N*, which agrees well with Fig. 2. In

ACCEPTED MANUSCRIPT

addition, as for the case of ac magnetization, an excess field $H_e(f)$ related to the eddy-current loss has to be taken into account. So the equation (3) can be modified as follows,

$$H_{nuc}^{N} = = H_{nuc}^{1} + (N-1)\cdot H_{i,j} + H_e(f) \qquad (4)$$

Fig. 6 shows the excess field $H_e(f)$ and the dipolar field $H_{i,j}$ (denoted by S) vary with frequency at driving current of 2 mA. The $H_e(f)$ can be obtained by curve fitting, basically following $H_e \sim f^{0.38}$ in our measurement range. The index closed to 0.5 indicates that the eddy-current loss mainly results from domain wall dynamics [28]. The non-linear trend after 4 MHz could be the consequence of higher frequency inhibiting domain wall dynamics. According to equation (4), the value of H_{nuc}^{N} becomes larger with increasing the number of ribbons and the driving frequency, giving rise to the decrease of the effective permeability μ_{eff} of the sample. Therefore, the characteristic frequency in Fig. 3 then shifts to higher frequency according to the relationship $f_c \propto 1/\pi\mu_{eff} t^2 \sigma$ [36], where t is the ribbon thickness.

Moreover, it can be seen from Fig. 6 that the frequency has slight influence on the dipolar interaction. The variation of dipolar field with frequency follows $H_{i,j} \sim f^{-0.06}$. The slight decrease of the dipolar field $H_{i,j}$ with increasing frequency could be observed as the result of sweeping rate $\mathrm{d}h_\varphi/\mathrm{d}t$ affecting the formation of dipolar field. When the rise time of the driving field is close to the formation time of dipolar field, the influence of the dipolar field decreases [37] and $H_{i,j}$ reduced accordingly. At driving frequency of 10 kHz, $H_{i,j}$ is fitted to be about 0.69 Oe. Furthermore, $K_{i,j}$ of 5.60×10^{-5} can be estimated by using M_i value of 1.24 T [38].

ACCEPTED MANUSCRIPT

Finally, Fig. 7 shows the influence of ac driving current on the nucleation field. The nucleation field decreased with the increasing of the value of driving current, which is related to the principle of minimum energy. It varied only about 0.08 Oe as the current change from 0.3 mA to 3 mA, as shown in Fig. 7b. Although the nucleation field didn't change obviously, the variation of $(\Delta Z/Z)_{max}$ was significant in Fig. 7a because μ_{eff} increased due to the reduced effective anisotropy. In other words, it also shows that the magneto-impedance effect is a sensitive tool for magnetism research.

4. Conclusion

In summary, we have investigated the dipolar interaction in the system of multiple FINEMET ribbons. The dipolar fields superimposed on the nucleation field of an arbitrary ribbon was measured and linearly increased with increasing the surrounding ribbons. It essentially changes the domain nucleation process, or the effective permeability under the combination of ac field and dc field. Besides, it apparently expands the "bell" magneto impedance spectra and raises its characteristic frequency. When the external field approaches or exceeds the nucleation field, each ribbon is simply treated as a dipole and the dipolar field is estimated accordingly. The influence of the ac current frequency on the nucleation field causes the increase of the nucleation field by eddy-current effect, whereas it has little effect on the dipolar field. The effect of the alternating field produced by the ac current reduces the nucleation field insignificantly, while the magneto-impedance ratio changes obviously. The results show that the magneto impedance effect is a very sensitive tool for investigation of magnetic materials and facilitate the design of the materials for

ACCEPTED MANUSCRIPT

magnetic devices.

Acknowledgments

This work is supported by the National Natural Science Foundation of China (11574084, 11774091 and 51572086).

ACCEPTED MANUSCRIPT

ACCEPTED MANUSCRIPT

Reference

[1] Y. Wang, W.H. Shi, H.X. Wei, D. Atkinson, B.S. Zhang, X.F. Han, Manipulation of magnetization reversal of $Ni_{81}Fe_{19}$ nanoellipse arrays by tuning the shape anisotropy and the magnetostatic interactions, Journal of Applied Physics, 111 (2012) 07B909. DOI: 10.1063/1.4895708

[2] Y. Velazquez-Galvan, J.M. Martinez-Huerta, L. Medina Jde, Y. Danlee, L. Piraux, A. Encinas, Dipolar interaction in arrays of magnetic nanotubes, Journal of physics: Condensed Matter, 26 (2014) 026001. DOI: 10.1088/0953-8984/26/2/026001

[3] P. Bender, F. Krämer, A. Tschöpe, R. Birringer, Influence of dipolar interactions on the angular-dependent coercivity of nickel nanocylinders, Journal of Physics D: Applied Physics, 48 (2015) 145003. DOI: 10.1088/0022-3727/48/14/145003

[4] W.B. Cui, H. Sepehri-Amin, Y.K. Takahashi, K. Hono, Hard magnetic properties of spacer-layer-tuned NdFeB/Ta/Fe nanocomposite films, Acta Materialia, 84 (2015) 405. DOI: 10.1016/j.actamat.2014.10.008

[5] Z.M. Dai, W. Liu, X.T. Zhao, Z. Han, D. Kim, C.J. Choi, Z.D. Zhang, Magnetic interactions in anisotropic Nd-Dy-Fe-Co-B/α-Fe multilayer magnets, Journal of Applied Physics, 120 (2016) 163906. DOI: 10.1063/1.4904411

[6] K.J. Kirk, J.N. Chapman, C.D.W. Wilkinson, Switching fields and magnetostatic interactions of thin film magnetic nanoelements, Applied Physics Letters, 71 (1997) 539. DOI: 10.1063/1.119602

[7] C. Lei, J. Lei, Z. Yang, Y. Zhou, Improved micro fluxgate sensor with double-layer Fe-based amorphous core, Microsystem Technologies, 19 (2013) 167. DOI: 10.1007/s00542-012-1523-z

[8] P. Ripka, X.P. Li, J. Fan, Multiwire core fluxgate, Sensors and Actuators A: Physical, 156 (2009) 265. DOI: 10.1016/j.sna.2009.06.006

[9] R. Piccin, D. Laroze, M. Knobel, P. Vargas, M. Vázquez, Magnetostatic interactions between two magnetic wires, Europhysics Letters , 78 (2007) 67004. DOI: 10.1209/0295-5075/78/67004

[10] H.L. Pan, X. Li, Q. Zhang, J.T. Wang, W.H. Xie, Z.J. Zhao, Dipole–dipole

ACCEPTED MANUSCRIPT

interaction in electronic article surveillance system, Journal of Physics D: Applied Physics, 50 (2017) 305002. DOI: 10.1088/1361-6463/aa754c

[11] A. Encinas-Oropesa, M. Demand, L. Piraux, I. Huynen, U. Ebels, Dipolar interactions in arrays of nickel nanowires studied by ferromagnetic resonance, Physical Review B, 63 (2001) 104415. DOI: 10.1103/PhysRevB.63.104415

[12] Q.F. Zhan, J.H. Gao, Y.Q. Liang, N.L. Di, Z.H. Cheng, Dipolar interactions in arrays of iron nanowires studied by Mössbauer spectroscopy, Physical Review B, 72 (2005) 024428-1. DOI: 10.1103/PhysRevB.72.024428

[13] L.C. Sampaio, E.H.C.P. Sinnecker, G.R.C. Cernicchiaro, M. Knobel, M. Vázquez, J. Velázquez, Magnetic microwires as macrospins in a long-range dipole-dipole interaction, Physical Review B, 61 (2000) 8976. DOI: 10.1103/PhysRevB.61.8976

[14] D. Laroze, J. Escrig, P. Landeros, D. Altbir, M. Vázquez, P. Vargas, A detailed analysis of dipolar interactions in arrays of bi-stable magnetic nanowires, Nanotechnology, 18 (2007) 415708. DOI: 10.1088/0957-4484/18/41/415708

[15] M. Rivas, J.C. Martínezgarcía, I. Škorvánek, J. Marcin, P. Švec, P. Gorria, Magnetostatic interaction in soft magnetic bilayer ribbons unambiguously identified by first-order reversal curve analysis, Applied Physics Letters, 107 (2015) 132403. DOI: 10.1063/1.4932066

[16] A. Chizhik, J. Gonzalez, A. Zhukov, J.M. Blanco, Interaction between Co-rich glass-covered microwires, Journal of Physics D: Applied Physics, 36 (2003) 1058. DOI: 10.1088/0022-3727/36/9/302

[17] S. Vock, K. Tschulik, M. Uhlemann, C. Hengst, S. Fähler, L. Schultz, V. Neu, Magnetostatic nearest neighbor interactions in a $Co_{48}Fe_{52}$ nanowire array probed by in-field magnetic force microscopy, Journal of Applied Physics, 118 (2015) 233901. DOI: 10.1063/1.4937275

[18] W. Zhao, X. Bu, G. Yu, C. Xiang, Feedback-type giant magneto-impedance sensor based on longitudinal excitation, Journal of Magnetism and Magnetic Materials, 324 (2012) 3073. DOI: 10.1016/j.jmmm.2012.05.004

[19] J. Devkota, T. Luong, J.S. Liu, H. Shen, F.X. Qin, J.F. Sun, P. Mukherjee, H. Srikanth, M.H. Phan, A soft ferromagnetic multiwire-based inductance coil sensor for

ACCEPTED MANUSCRIPT

sensing applications, Journal of Applied Physics, 116 (2014) 234504. DOI: 10.1063/1.4904411

[20] G.V. Kurlyandskaya, E. Fernández, A. Svalov, A.B. Beitia, A. García-Arribas, A. Larrañaga, Flexible thin film magnetoimpedance sensors, Journal of Magnetism and Magnetic Materials, 415 (2016) 91. DOI: 10.1016/j.jmmm.2016.02.004

[21] Y. Han, X. Li, W.X. Lv, W.H. Xie, Q. Zhao, Z.J. Zhao, Magnetoimpedance effect of FINEMET ribbons coated with $Fe_{20}Ni_{80}$ permalloy film, Journal of Alloys and Compounds, 678 (2016) 494. DOI: 10.1016/j.jallcom.2016.04.021

[22] L. Jamilpanah, M.R. Hajiali, S.M. Mohseni, S. Erfanifam, S.M. Mohseni, M. Houshiar, S.E. Roozmeh, Magnetoimpedance exchange coupling in different magnetic strength thin layers electrodeposited on Co-based magnetic ribbons, Journal of Physics D: Applied Physics, 50 (2017) 155001. DOI: 10.1088/1361-6463/aa6098

[23] R.L. Sommer, C.L. Chien, Longitudinal and transverse magneto-impedance in amorphous $Fe_{73.5}Cu_1Nb_3Si_{13.5}B_9$ films, Applied Physics Letters, 67 (1995) 3346. DOI: 10.1063/1.115242

[24] J.X. Yang, X.L. Yang, G. Chen, B.Y. Hu, G.T. Shen, K.Y. Jiang, Magneto-impedance effect in soft Fe-based nanocrystalline alloys, Chinese Science Bulletin, 42 (1997) 196. DOI: 10.1007/BF02882433

[25] K. Mohri, T. Kohsawa, K. Kawashima, H. Yoshida, Magneto-inductive effect (MI effect) in amorphous wires, IEEE Transactions on Magnetics, 28 (1992) 3150. DOI: 10.1109/20.17974

[26] A. Zhukov, M. Vázquez, J. Velázquez, C. García, R. Valenzuela, B. Ponomarev, Frequency dependence of coercivity in rapidly quenched amorphous materials, Materials Science and Engineering A, s226–228 (1997) 753. DOI: 10.1016/S0921-5093(97)80079-2

[27] Z.C. Wang, F.F. Gong, X.L. Yang, L. Zeng, G. Chen, J.X. Yang, S.M. Qian, D.P. Yang, Longitudinally driven giant magnetoimpedance effect in stress-annealed Fe-based nanocrystalline ribbons, Journal of Applied Physics, 87 (2000) 4819. DOI: 10.1063/1.373170

[28] Y.F. Li, P. Liu, X.M. Zhao, Y. Meng, P.Y. Chen, Q.H. Liu, Circular magnetization

ACCEPTED MANUSCRIPT

and energy loss in Fe-based soft magnetic wires, Journal of Magnetism and Magnetic Materials, 349 (2014) 100. DOI: 10.1016/j.jmmm.2013.08.055

[29] M.H. Phan, H.X. Peng, Giant magnetoimpedance materials: Fundamentals and applications, Progress in Materials Science, 53 (2008) 323. DOI: 10.1016/j.pmatsci.2007.05.003

[30] M.H. Phan, H.X. Peng, S.C. Yu, M.R. Wisnom, Large enhancement of GMI effect in polymer composites containing Co-based ferromagnetic microwires, Journal of Magnetism and Magnetic Materials, 316 (2007) e253. DOI: 10.1016/j.jmmm.2007.02.112

[31] E.F. Silva, M. Gamino, A.M.H. de Andrade, M.A. Corrêa, M. Vázquez, F. Bohn, Tunable asymmetric magnetoimpedance effect in ferromagnetic NiFe/Cu/Co films, Applied Physics Letters, 105 (2014) 102409. DOI: 10.1063/1.4895708

[32] J. Fan, J. Wu, N. Ning, H. Chiriac, X. Li, Magnetic Dynamic Interaction in Amorphous Microwire Array, IEEE Transactions on Magnetics, 46 (2010) 2431. DOI: 10.1109/tmag.2010.2044378

[33] X.L. Yang, J.X. Yang, G. Chen, G.T. Shen, B.Y. Hu, K.Y. Jiang, Magneto-impedance effect in field- and stress-annealed Fe-based nanocrystalline alloys, Journal of Magnetism and Magnetic Materials, 175 (1997) 285. DOI: 10.1016/S0304-8853(97)00210-2

[34] Y.F. Li, M. Vázquez, S.Z. Yin, Frequency- and axial-field-dependent circular magnetization reversal in a stress-annealed Fe-based nanocrystalline wire, Journal of Magnetism and Magnetic Materials, 321 (2009) 1111. DOI: 10.1016/j.jmmm.2008.10.021

[35] E. Fernández, A.V. Svalov, G.V. Kurlyandskaya, A. Garcia-Arribas, GMI in Nanostructured FeNi/Ti Multilayers With Different Thicknesses of the Magnetic Layers, IEEE Transactions on Magnetics, 49 (2013) 18. DOI: 10.1109/TMAG.2012.2218221

[36] P. Jantaratana, C. Sirisathitkul, Effects of thickness and heat treatments on giant magnetoimpedance of electrodeposited cobalt on silver wires, IEEE Transactions on Magnetics, 42 (2006) 358. DOI: 10.1109/TMAG.2005.863270

ACCEPTED MANUSCRIPT

[37] A. Chizhik, A. Zhukov, J.M. Blanco, R. Szymczak, J. Gonzalez, Interaction between Fe-rich ferromagnetic glass-coated microwires, Journal of Magnetism and Magnetic Materials, 249 (2002) 99. DOI: 10.1016/S0304-8853(02)00513-9

[38] Y. Yoshizawa, S. Oguma, K. Yamauchi, New Fe-based soft magnetic alloys composed of ultrafine grain structure, Journal of Applied Physics, 64 (1988) 6044. DOI: 10.1063/1.342149

ACCEPTED MANUSCRIPT

ACCEPTED MANUSCRIPT

Figure caption

Fig. 1 LDMI ratio in variation with the external magnetic field for *N* pieces of FINEMET ribbons at various frequencies, *i*=2 mA.

Fig. 2 The dependence of field $H_{\mathrm{nuc}}^{\mathrm{N}}$ on the number of FINEMET ribbons at various frequencies, *i*=2mA.

Fig. 3 Frequency dependence of the maximum of LDMI ratio $(\Delta Z/Z)_{max}$ for $(F)_N$ at driven current *i*=2 mA. The inset shows the case at 35~550 kHz.

Fig. 4 The longitudinal hysteresis loops of different number of FINEMET ribbons. The inset shows that the anisotropy field $H_{\mathrm{k}}^{\mathrm{N}}$ varies with *N*.

Fig. 5 Schematic description of magnetization in a FINEMET ribbon. Magnetization M_i, in the natural state of H_{ex}=0 Oe (a), the unsaturated sate of $H_{\mathrm{ex}}<H_{\mathrm{nuc}}^{\mathrm{N}}$ (b), and the saturated sate of $H_{\mathrm{ex}} \geq H_{\mathrm{nuc}}^{\mathrm{N}}$ (c).

Fig. 6 H_{e} and S vary with frequency, *i*=2 mA. S and H_{e} represent for the slope of $H_{\mathrm{nuc}}^{\mathrm{N}}(N)$ fitting line and the excess term related to the eddy-current loss.

Fig. 7 (a) LDMI ratio in variation with the external magnetic field for a FINEMET ribbon at various driven current, *f*=10 kHz. The inset shows the case at ±1.25 Oe. (b) The field H_{nuc}^{1} dependence of the driven currents at frequency of 10 kHz.

ACCEPTED MANUSCRIPT

ACCEPTED MANUSCRIPT

Figure 1

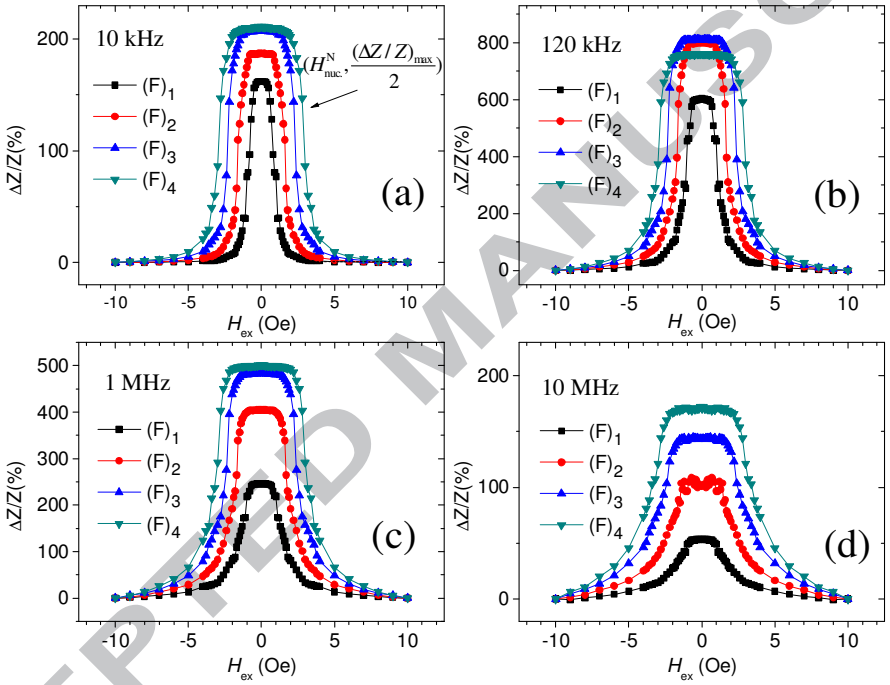

ACCEPTED MANUSCRIPT

ACCEPTED MANUSCRIPT

Figure 2

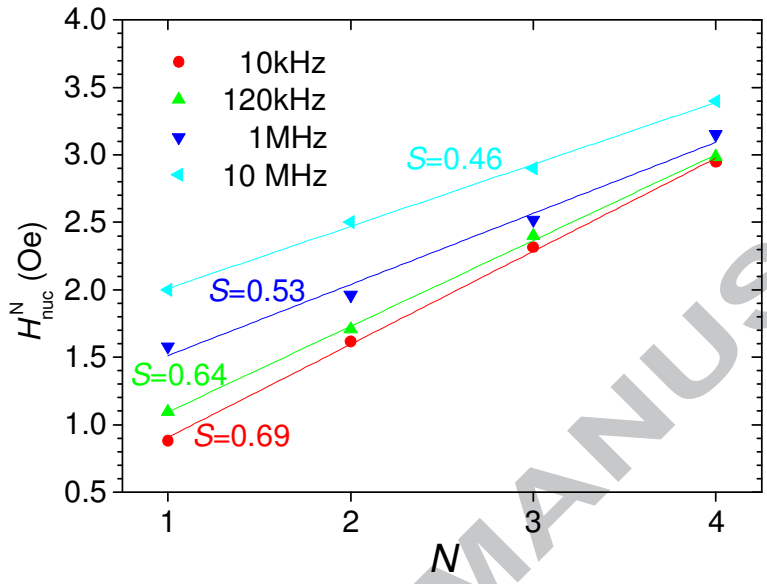

ACCEPTED MANUSCRIPT

ACCEPTED MANUSCRIPT

Figure 3

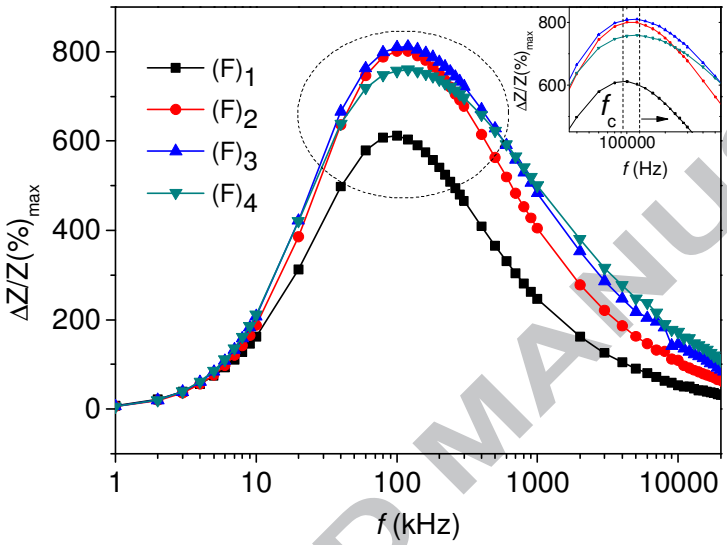

ACCEPTED MANUSCRIPT

ACCEPTED MANUSCRIPT

Figure 4

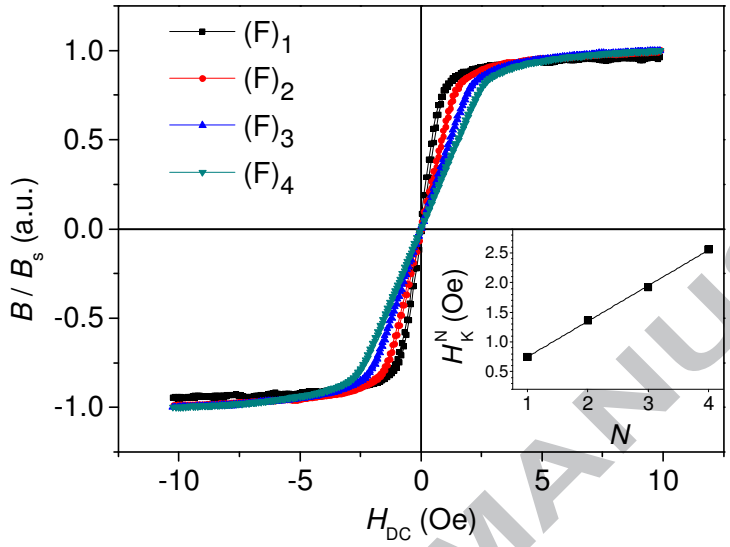

ACCEPTED MANUSCRIPT

ACCEPTED MANUSCRIPT

Figure 5

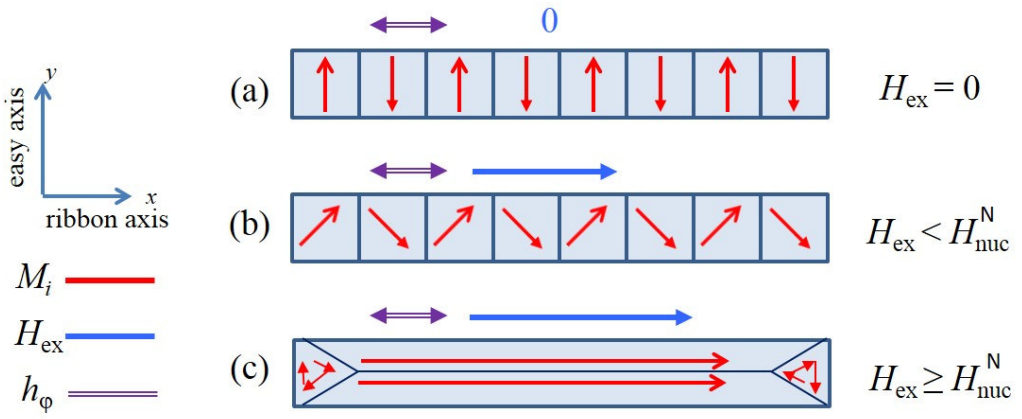

ACCEPTED MANUSCRIPT

ACCEPTED MANUSCRIPT

Figure 6

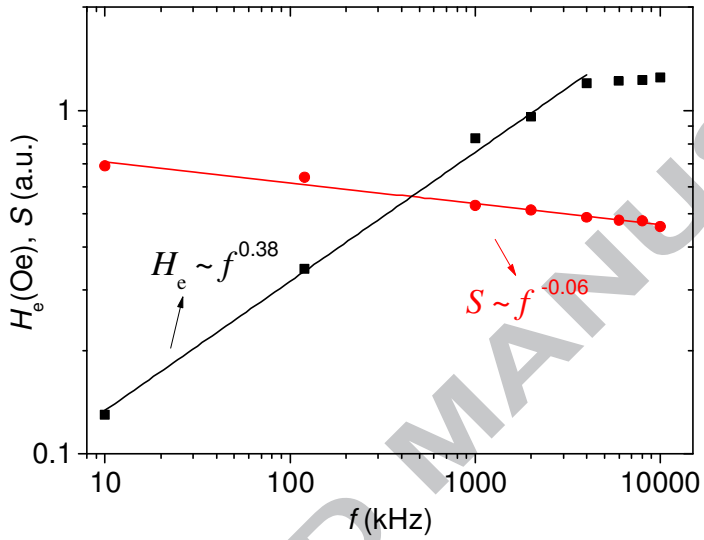

ACCEPTED MANUSCRIPT

ACCEPTED MANUSCRIPT

Figure 7

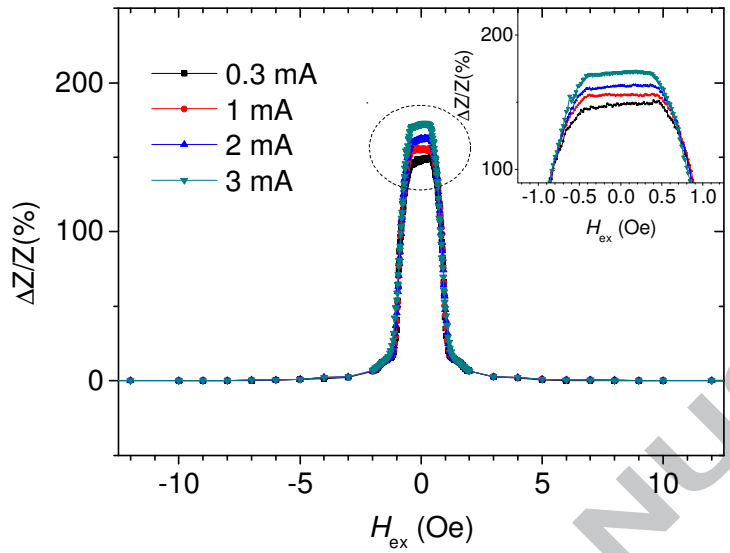

(a)

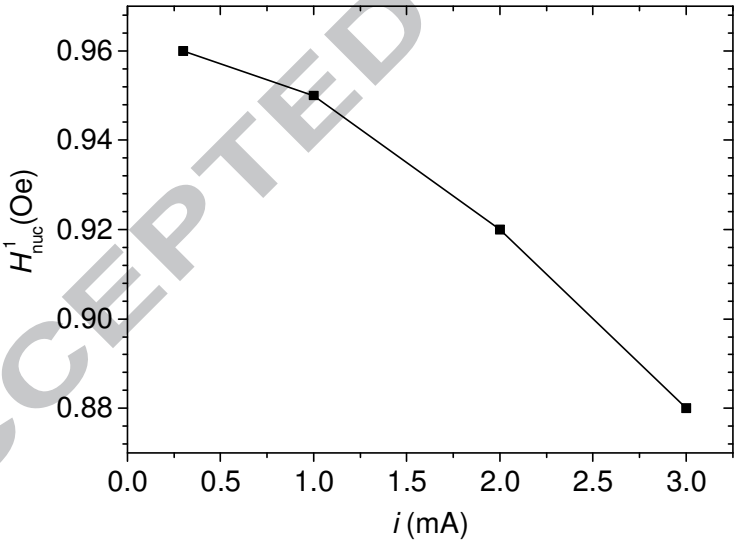

(b)

ACCEPTED MANUSCRIPT

ACCEPTED MANUSCRIPT

Highlights

GMI effect is a sensitive tool to study the magnetic properties of the multi ribbons.

The dipole-dipole interaction will modify the magnetic properties of the FINEMET ribbons.

To design a magnetic device, the influence of the dipole-dipole interaction has to be thought about.

ACCEPTED MANUSCRIPT